Supplementary Material

1. Characterisation

2. Seasonal field monitoring

List of Notation

L_0		Densitometer reading at the base of the central rod before soil excavation
L_1		Densitometer reading at the base of the central rod after excavated volume is filled with water
V	→	Volume of soil excavated in densitometer test up to 20 cm depth
D_i	→	i% of the particles are finer than this size
EC-5	→	Capacitance sensor, Decagon Devices
TDR	→	Time domain reflectometry sensor, Campbell Scientific
10HS	→	Capacitance sensor, Decagon Devices
GSD	→	Grain size distribution
GPR	→	Ground penetrating radar
IGT	→	Institute for geotechnical engineering
IT	→	Instrumented Trench
VWC	→	Volumetric water content
R^2	→	R-square or coefficient of determination

1. Characterisation

1.1 Soil unit weight: Balloon method device (MagdeBurger Prüfgeräte GmbH (HMP), DIN 18125-2:2011-03))

Procedure: A clean and flat surface was prepared for the support aluminium plate (designed by IGT), which contains the base ring (Figure S1(a)). Soil was excavated to 5 cm depth, removed and discarded. The densitometer (Figure S1(b)), containing approx. 6 litres of water (mixed with a lubricant to reduce piston friction), was placed on the base ring, and the piston was pushed until water filled the hole up to the two calibrating marks in the tube. The initial position L_0 was read, before the densitometer was removed and the soil was excavated to 20 cm depth, with walls as vertical as possible. The soil was stored and the measurement with densitometer L_1 was repeated. The volume of the bottom hole V is equal to the volume of liquid displaced by the device piston between the two readings L_0 and L_1 readings. The dry unit weight was determined using the calculated volume and the dry weight of the soil excavated.

Figure S1. Balloon method device used in in situ soil unit weight measurements in gravelly soil at the scree slope. (a): densitometer testing in a steep section of the slope with support plate at the base (IGT design); (b): densitometer set up near IT4.

1.2 Triaxial testing

1.2.1 Triaxial apparatus

The tests were carried out using two different triaxial apparatuses (a mid- and large scale) at the Institute for Geotechnical Engineering (IGT), ETH Zurich (Figure S2).

1.2.2 Mid-scale triaxial apparatus

The mid-scale triaxial (Figure S2(a)) is described in detail by Buchheister [1]. It consists of an adapted hollow cylinder apparatus in which a specimen with a diameter of 150 mm and a height of 300 mm can be placed inside a cylindrical pressure chamber, and loaded by a triaxial press. The apparatus is controlled electronically and is able to apply static and dynamic loads and to perform load-controlled tests (Table S1). Vertical forces and torques are applied by the use of two independent hydraulic cylinders. The applied force is measured by a load cell with a maximum of 63 kN. The displacement can reach a maximum of 100 mm and is measured by an integrated sensor within the hydraulic cylinders.

1.2.3 Large scale triaxial apparatus

The large scale triaxial apparatus (Figure S2(b)) is described by Guldenfels [2]. The electronically regulated system is able to apply static, quasi static, dynamic axial loads and to perform tests under controlled force or deformation. The axial load is transmitted by a hydraulic cylinder and measured by a load cell, with a maximum capacity of 160 kN. The axial deformation is measured by a sensor integrated within the hydraulic cylinder, with a maximum displacement of 100 mm. The specimen for this apparatus has a diameter of 250 mm, and a height of 500 mm.

Table S1. Specifications of the triaxial apparatuses.

Test	Type	Maximum axial displacement [mm]	Capacity of axial loading device [kN]	Diameter of specimen [mm]	Height of specimen [mm]
Mid-scale	HCA	±50	63	150	300
Large scale	Schenk	±50	160	250	500

Figure S2. Triaxial testing apparatuses. (a): mid-scale; (b): large scale, (photograph: R. Grob, 2015).

1.2.4 Grain size distribution post shearing

Figure S3 and Table S2 show the GSD after shearing, of a large triaxial testing sample. There is increase of the fine content percentage and in the sand fraction, which suggests the crushing of particles during testing at higher confining pressures.

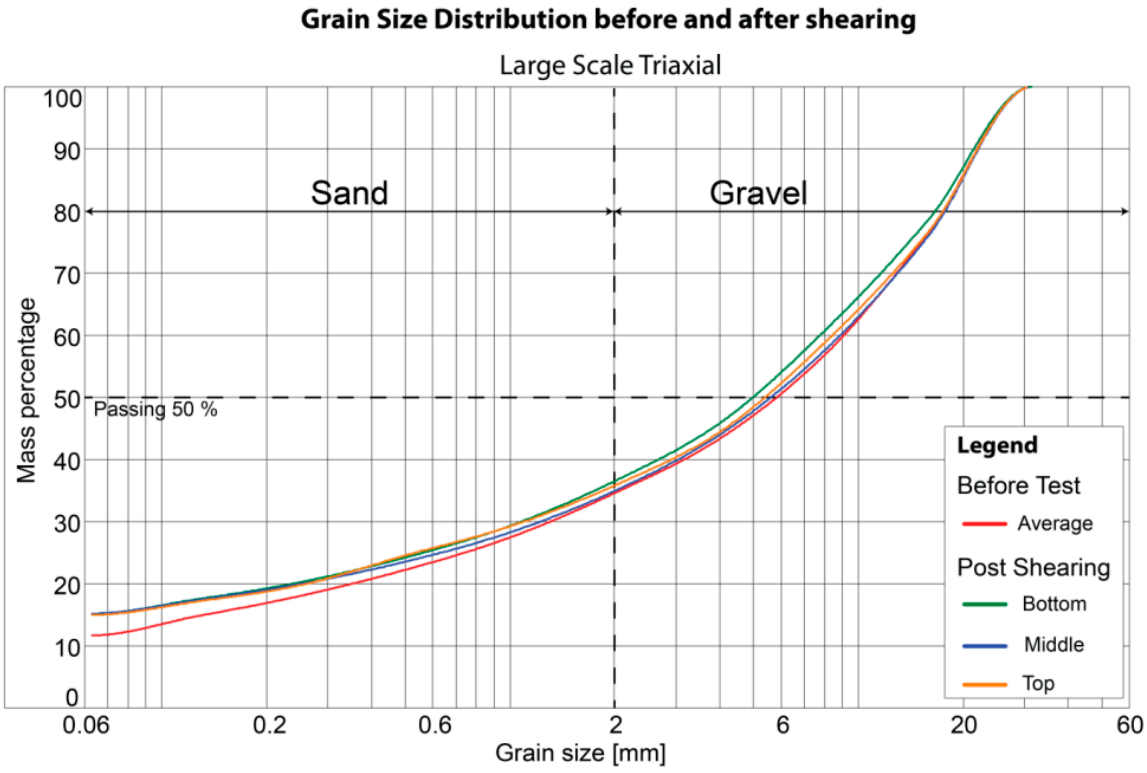

Figure S3. Grain size distribution before testing and after shearing for large scale test 3. The post-shearing curves from the bottom, middle and top of the specimen show the crushing of particles.

Table S2. Diameter D_i (i% of the particles are finer than this size) for large triaxial specimen before and after shearing.

D_i	Before [mm]	After [mm]		
	average	**Bottom**	**Middle**	**Top**
D_{30}	1.3	1.1	1.2	1.1
D_{50}	5.8	5.0	5.6	5.3

1.3 Ground Penetrating Radar (GPR).

An overview of all the relevant acquisition parameters used during GPR surveys are provided in Table S3 and S4.

Table S3. Overview of all acquisition parameters used during GPR surveys. "PE" stands for PulseEKKO, and "GB" for ground-based acquisition. The sampling interval was chosen as 0.4 ns, according to the specifications from the manufacturer. Two values are presented for the number of samples and the recorded time, as they were adjusted during the acquisition. Corresponding profile lines are shown in Figure 1(b).

System	**Type**	**Date** [dd.mm.yyyy]	**Frequency** [MHz]	**Temporal sampling interval** [ns]	**Number of samples/trace**	**Time window** [ns]	**Stacks**
PE	GB	15/16.05.2014	250	0.4	1000/625	400/250	8

Table S4 gives an overview of all processing steps that were applied for GPR data, including the most important selected parameters, selection criteria and amounts of eliminated data. GPR data from ground-based acquisition were processed using the same workflow, including all processing steps, which are commonly applied to GPR data [3-5].

Table S4. Selected processing parameters for each GPR acquisition.

System	Type	Selected time window [ns]	Band Pass Filter [MHz]	Single value decomposition (SVD) filter length [ns]	Deconvolution filter length [ns]	Bin size [m]	Radar pulse velocity in soil [m/ns]
PE_{May14}	GB	200	100/600	30	20	0.05	0.1

2. Seasonal field monitoring

2.1 Calibration procedure

A site-specific recalibration was performed under laboratory-controlled conditions to determine VWC and to investigate the influence of the temperature variations in gravelly soil over a range of temperature of -6 °C- 23°C.

Samples were reconstituted in a rectangular box with base dimensions of 26x36cm (Figure S4), and with approximately 20 cm height, with soil collected from the field at each instrumented trench location. The dry unit weight from each IT1-4 was obtained from the in situ densitometer test, and used to reproduce the field conditions for each of the 4 laboratory samples.

The models were constructed with soil mixed homogeneously in four layers of 5 cm height. The TDR and capacitance sensors were inserted in the soil in horizontal and vertical directions, respectively allowing spacing between volumes of measurements. Air and soil temperature sensors, EC-5/10HS and TDR sensors were connected to the same data logger as in the field (Figures S4, S6).

Moisture content and temperature conditions were maintained for 10-15 minutes at each stage and the rate of data recording was 0.04 Hz. The moisture content of the soil was increased from 0, 1, 3, 5, 8 % up to saturation, and measurements were recorded at the following temperatures: ambient room (17 °C-23 °C), 10 °C, 1 °C and -5 °C.

After each measurement at a defined temperature, the water content was determined and water added to reach the VWC target (Figures S7-S14). Finally, a grain size analysis was performed on the four model samples, according to the Swiss standard classification (SN 670 004-2NA).

Some of the challenges and findings were:

- Sensor measurements indicate soil temperatures ranging from -5 °C to 23°C. Figures S7(a)-(f) show the recalibration data and equations for IT1, IT2 and IT4. Each row corresponded to the VWC measured with capacitance sensors (EC-5/10HS, left) and TDR (right), respectively, for the same trench. Each colour (blue, green, red) defines the target temperature (1°C, 10°C, room temperature), respectively. Data shown in orange corresponds to the initial calibration obtained using soil from IT1 with measurements at room temperature. The calibration equation to determine the VWC for each sensor was the best (linear or polynomial) fit to the data, with the highest value of R^2. The full record of data for each sensor in trenches (IT1-4) (S9-S14).
- Obtaining recalibration data from the coarser soil in IT3, since it was not possible to establish an appropriate unique relationship (in terms of achieving a suitable value R^2) between the VWC and measurements in the laboratory. It is not clear if that was due to the GSD or sensor damage.
- Noting the small variations between VWC measurements (EC-5/10HS and TDR) and temperatures (1 °C-23 °C) (Figure S7), which agree with the results by Topp [6], who had tested

TDRs in clay loam (10 °C-36 °C). Results reported by Davis [7] and Wobschall [8] for similar range of temperature variations (0 °C-30°C) in clay and laboratory selected soils respectively, show a small difference between readings at different temperatures at lower VWCs [9].

- A relationship between the dielectric constant increase/decrease with temperature was not found. Pepin [9] said the dielectric constant in TDRs decreased with increased temperature (in sand), while Bogena [10] found that the permittivity in EC-5 sensors increased with increasing temperature (in a water solution).
- Finally, remaining differences between sensor measurements could be due to discrepancies between measurement volume and installation depth [10]. An additional factor is due to sensor installation, since the EC-5/10HS were inserted vertically in the soil model in the laboratory to create less disturbance, whereas they were installed horizontally in the field; while the TDRs were calibrated and installed horizontally. This could have more influence on the 10HS because of the larger volume of influence during measurement, compared to the EC-5 sensors.

2.2 VWC sensor recalibration equation

Figure S8(a)-(f). shows a unique recalibration equation (in blue colour) for IT1, IT2 and IT4, which integrates all of the data presented in Figure S7 for temperatures >0°C. The advantage of this new recalibration over the original calibration (orange colour), is that these later measurements were performed with the soil excavated from the destination trench, and reconstituted at the void ratio measured in the field.

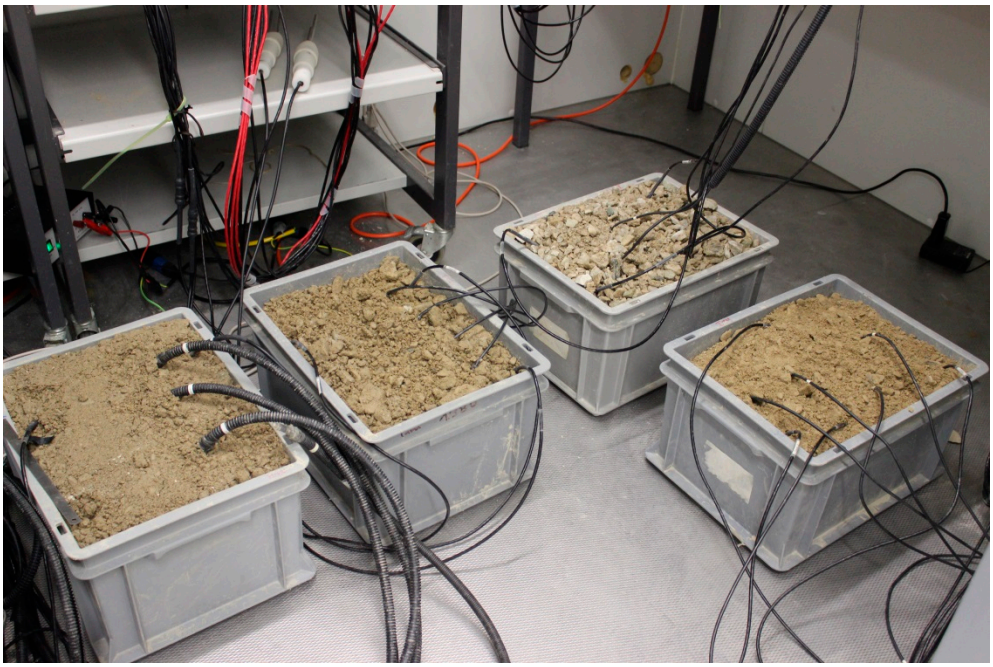

Figure S4. Soil in reconstituted samples for calibrating sensors from IT1-4.

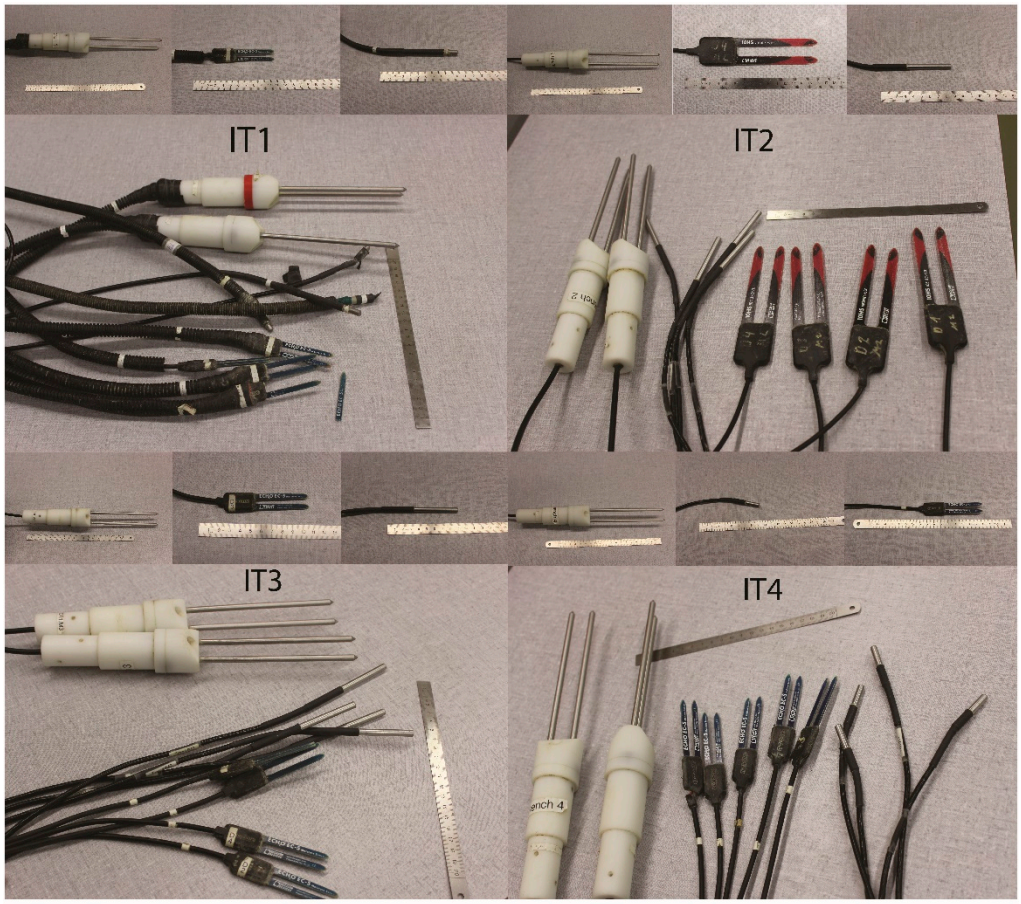

Figure S5. Sensors for each of the instrumented trenches IT1-4.

Figure S6. Controlled room temperature at IGT ETH Zürich.

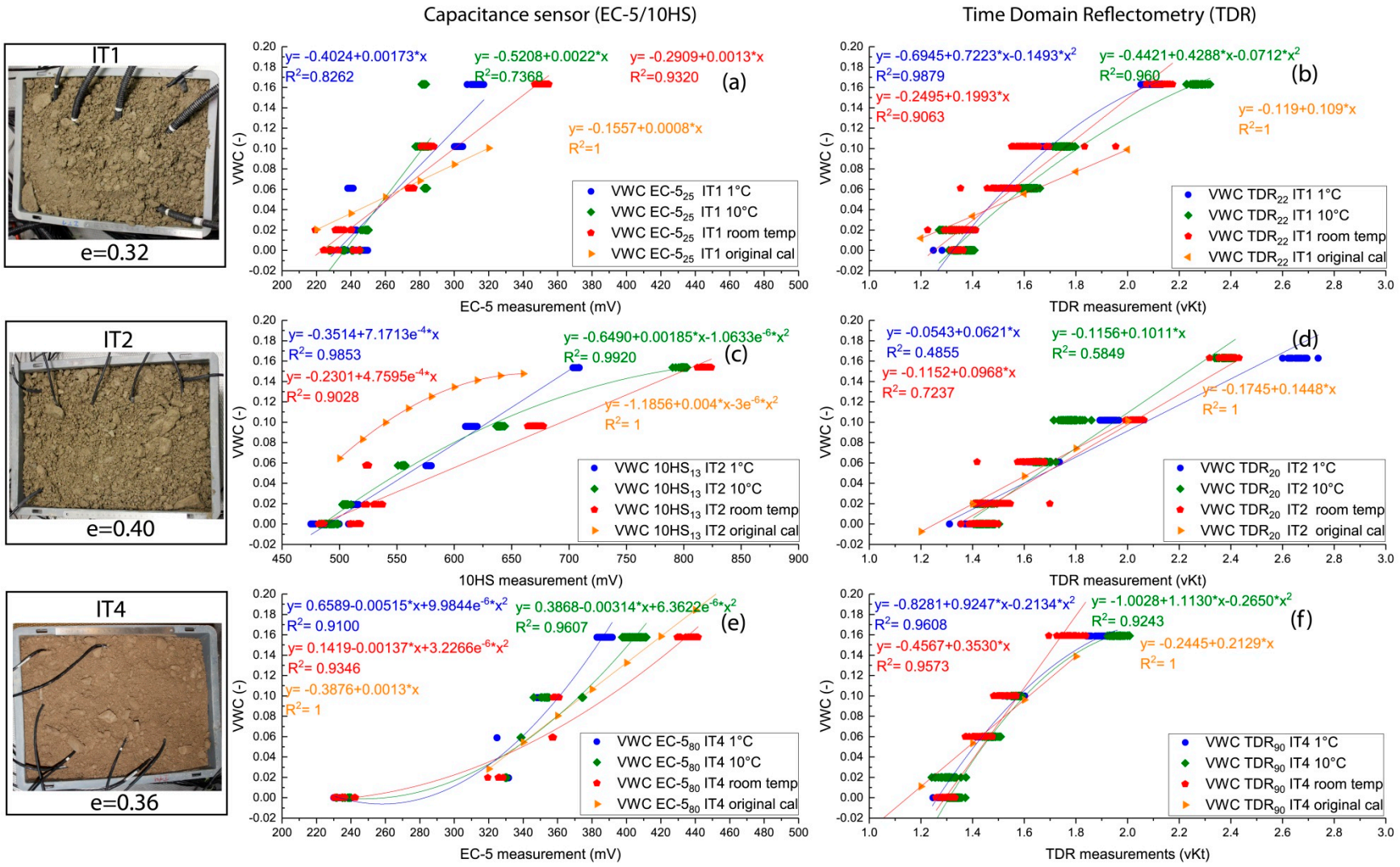

Figure S7. Site-specific calibration of VWC sensors of IT1, IT2, IT4 and the effect of temperature. With the exception of TDR in IT2 where R^2<0.5, all R^2 >0.82.

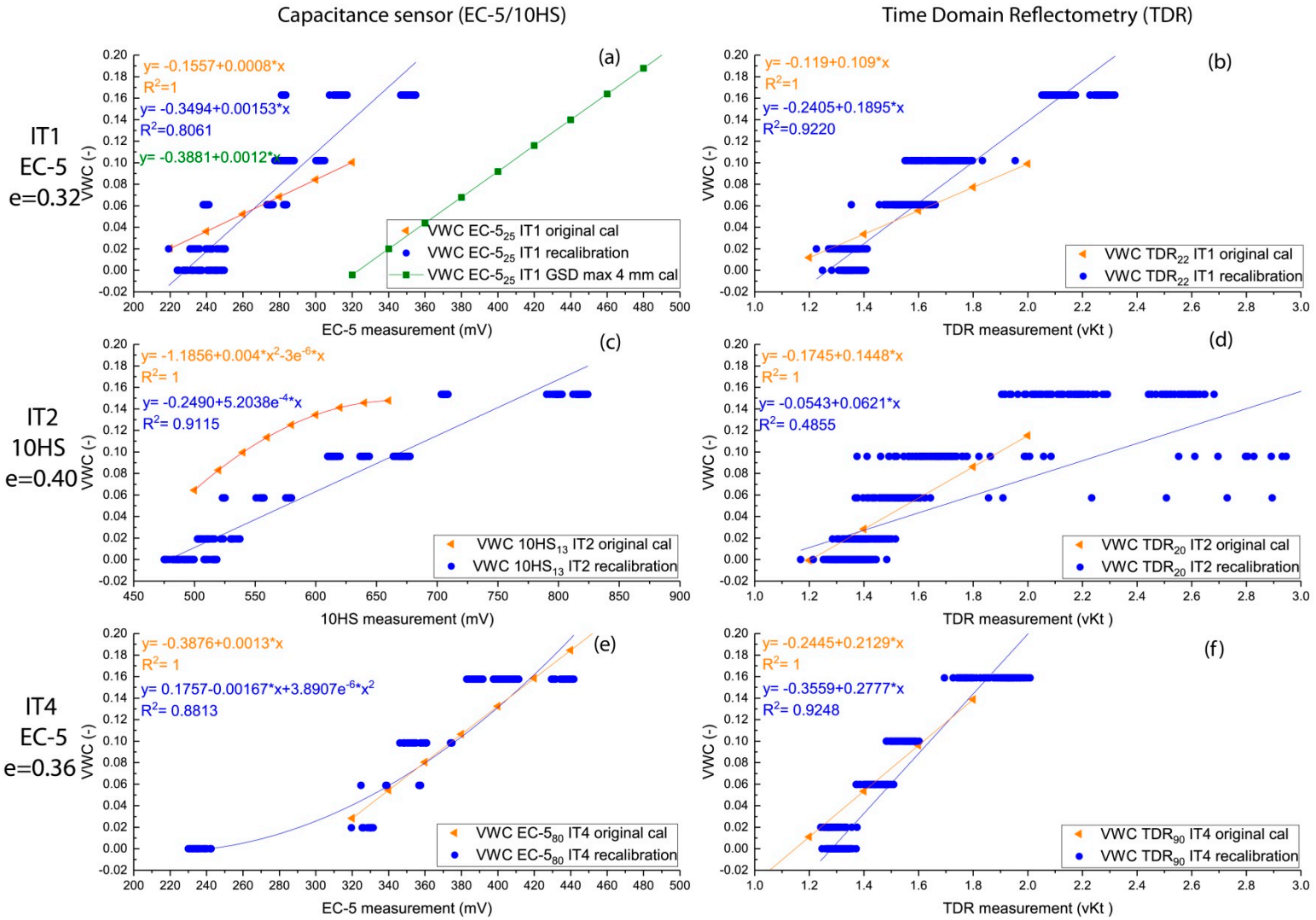

Figure S8. Site-specific calibration for IT1, IT2 and IT4. For a range of temperature (1 °C to 23 °C).

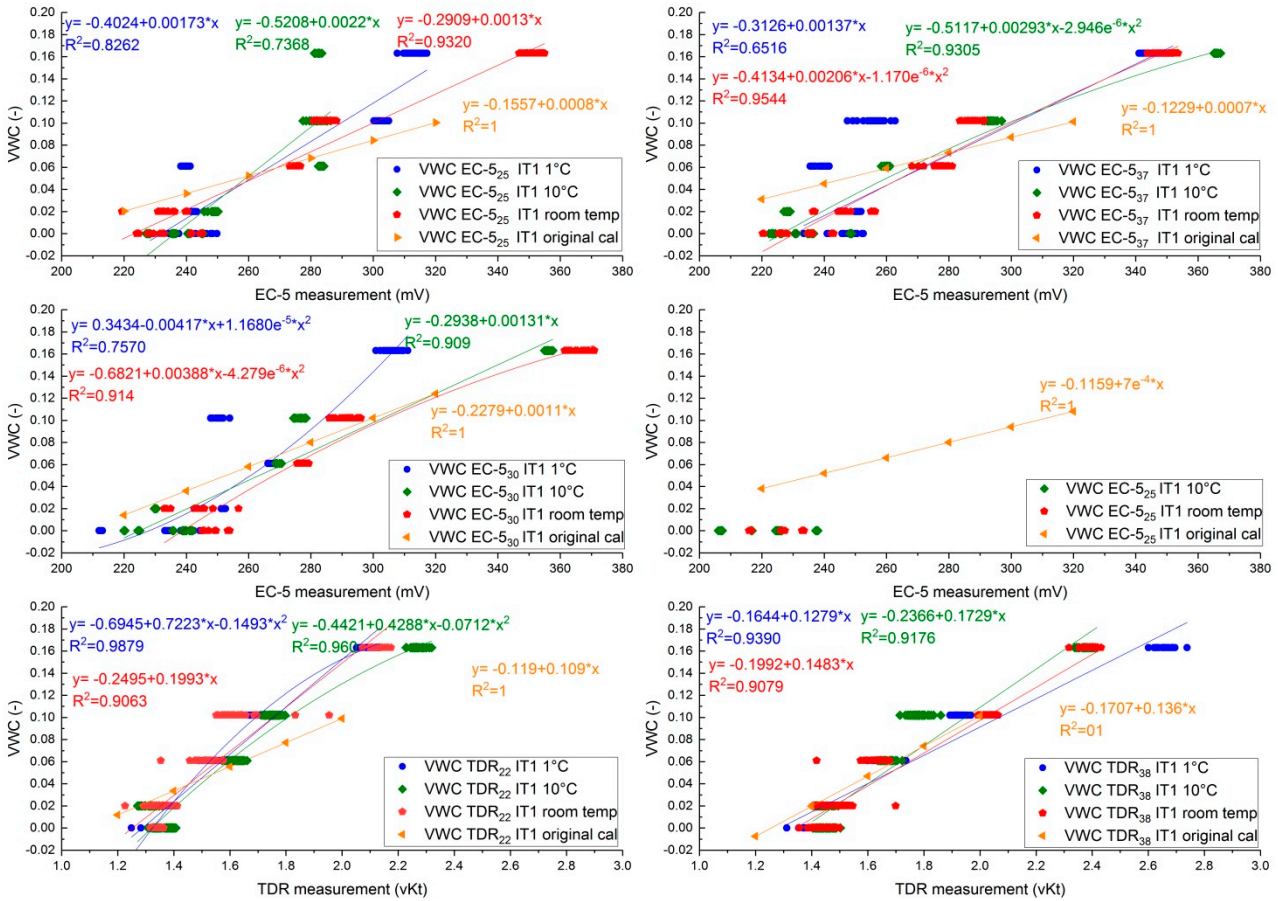

Figure S9. Site-specific calibration of TDR and EC-5 sensors in terms of temperature IT1.

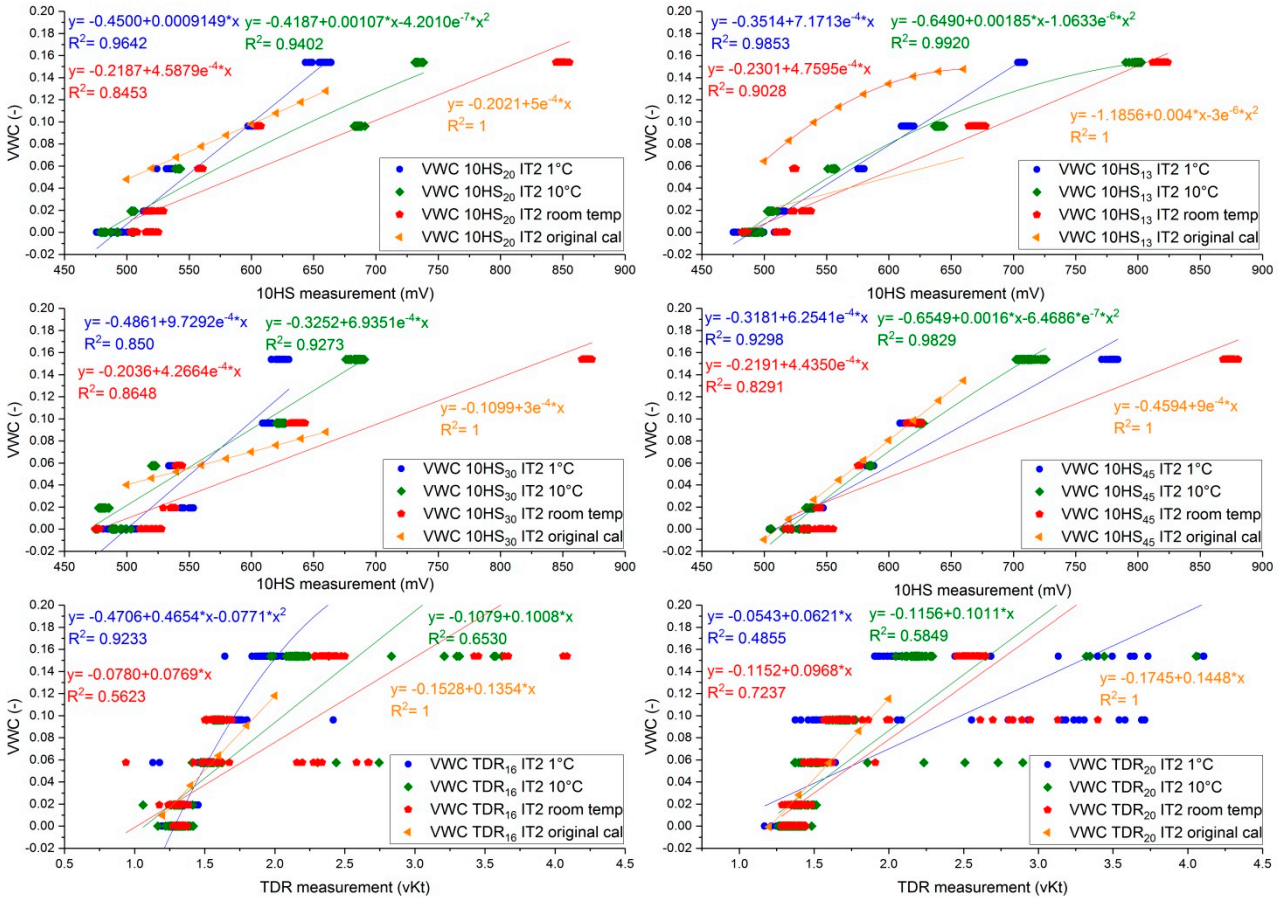

Figure S10. Site-specific calibration of TDR and 10HS sensors in terms of temperature, IT2.

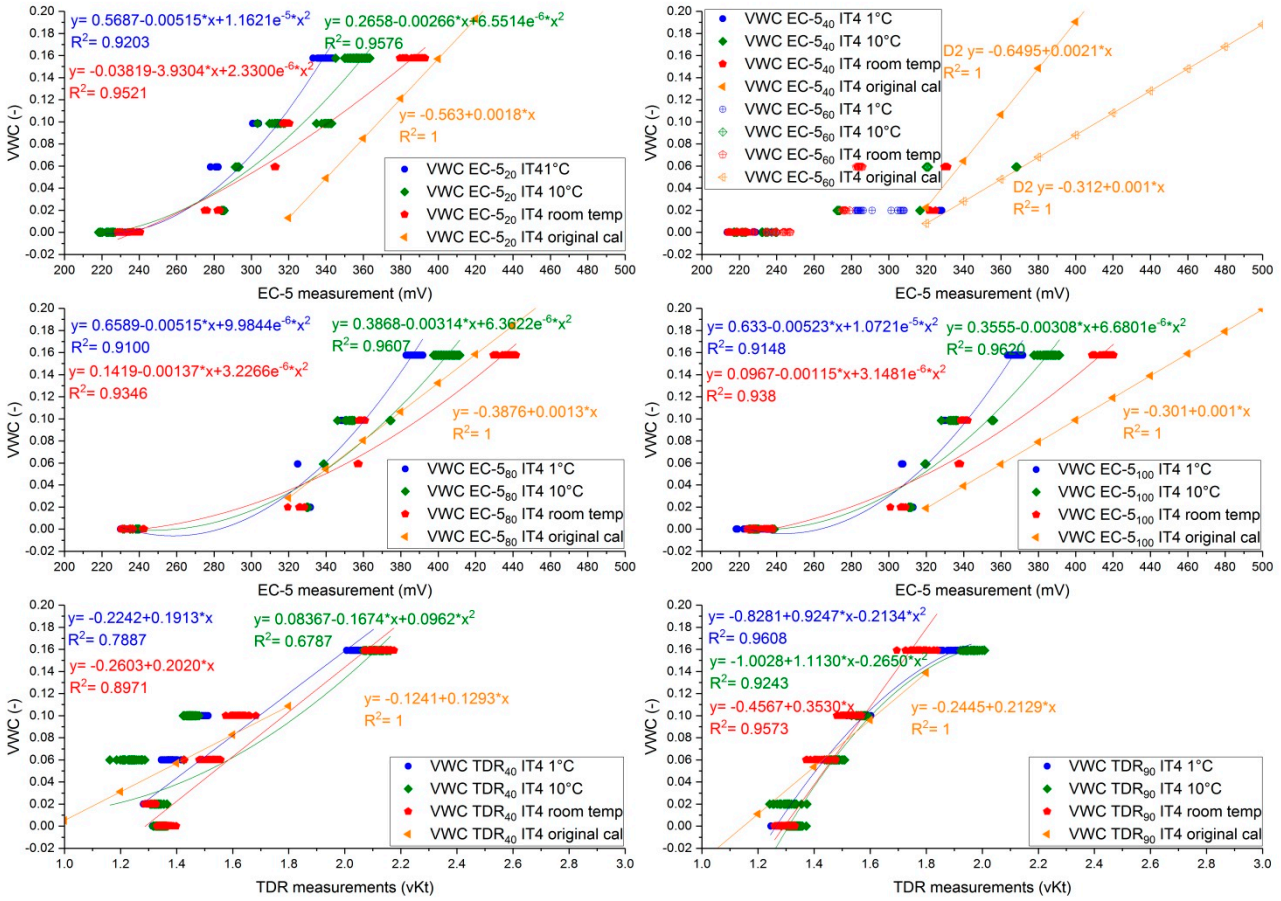

Figure S11. Site-specific calibration of TDR and EC-5 sensors in terms of temperature, IT4.

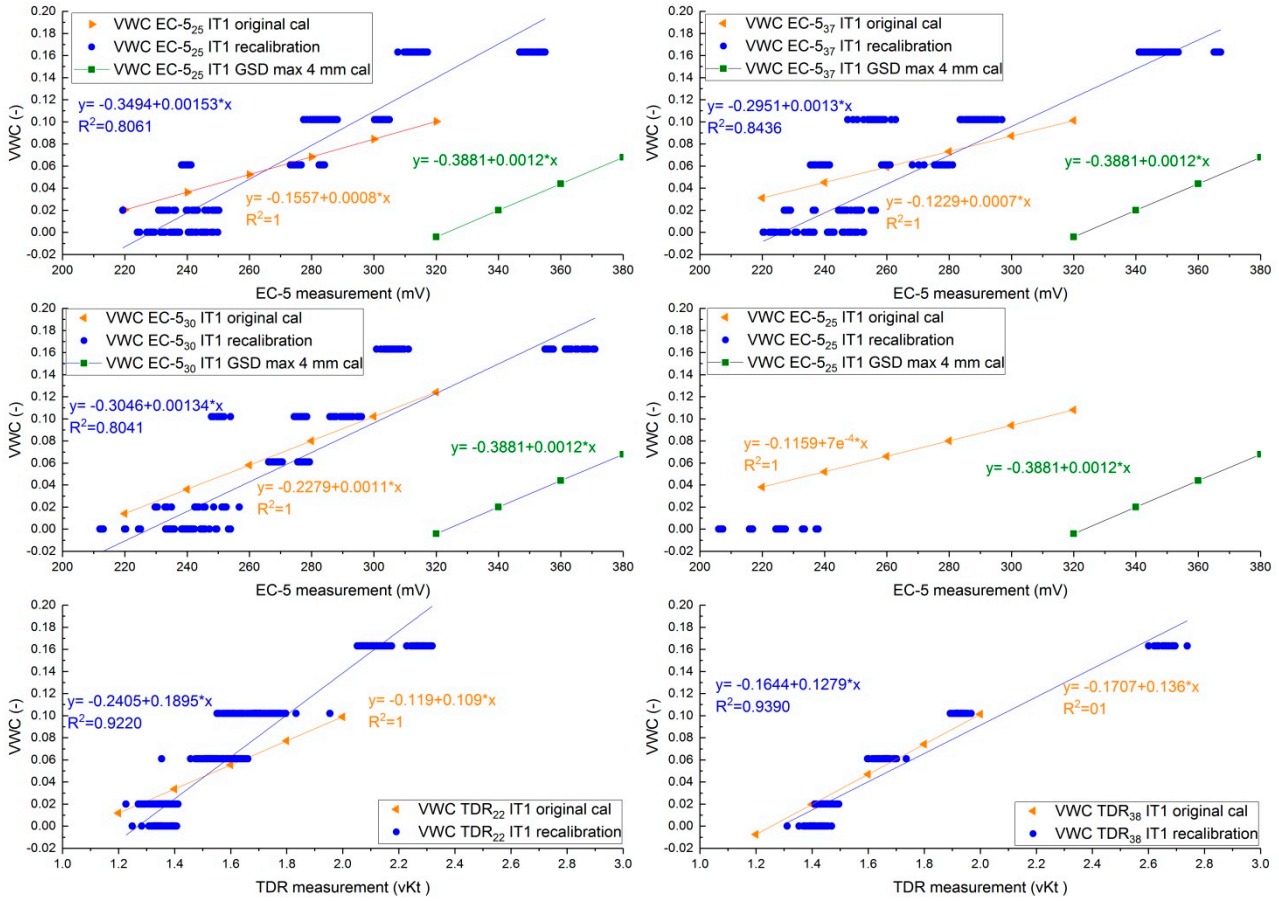

Figure S12. Site specific calibration for positive temperatures, IT1.

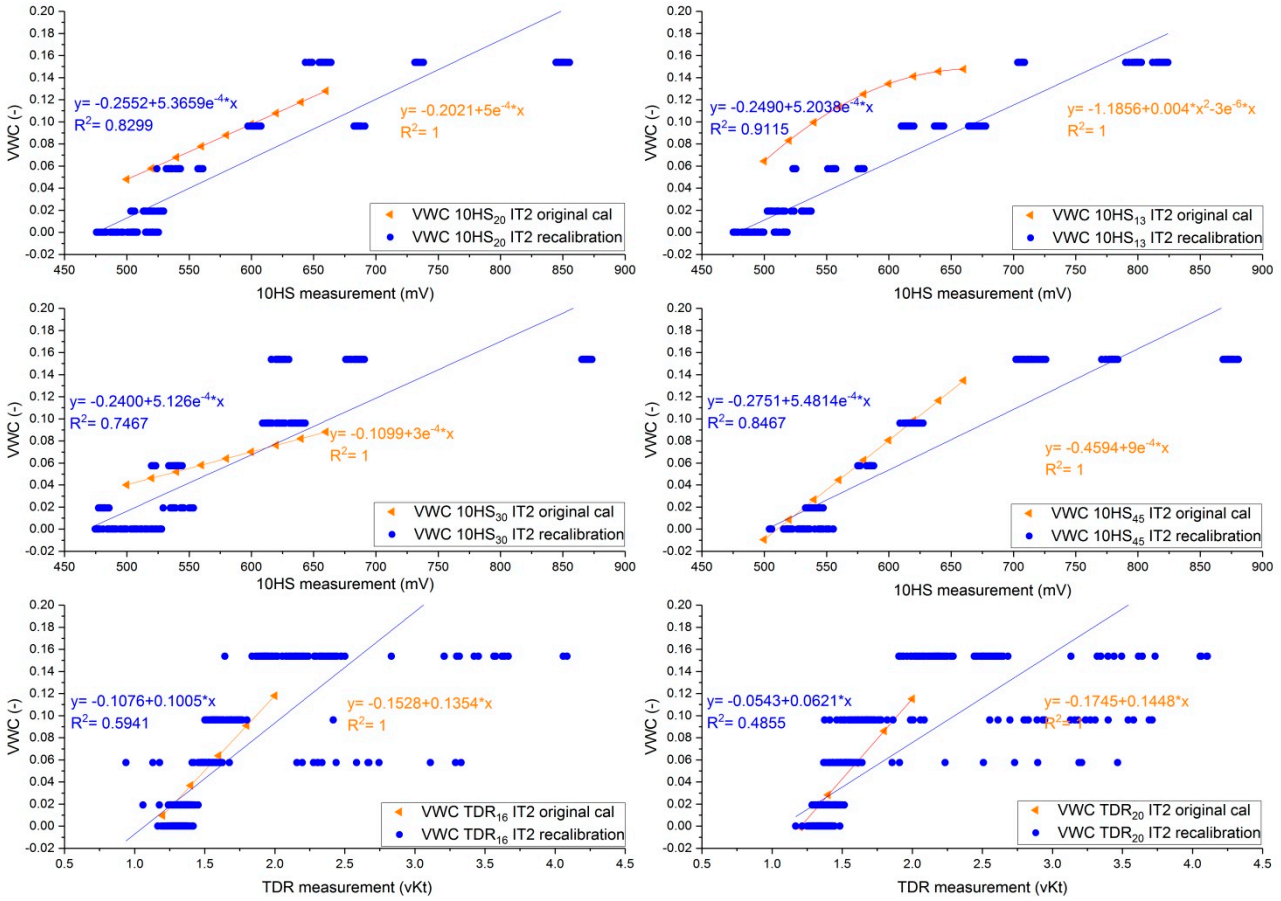

Figure S13. Site-specific calibration for positive temperatures, IT2.

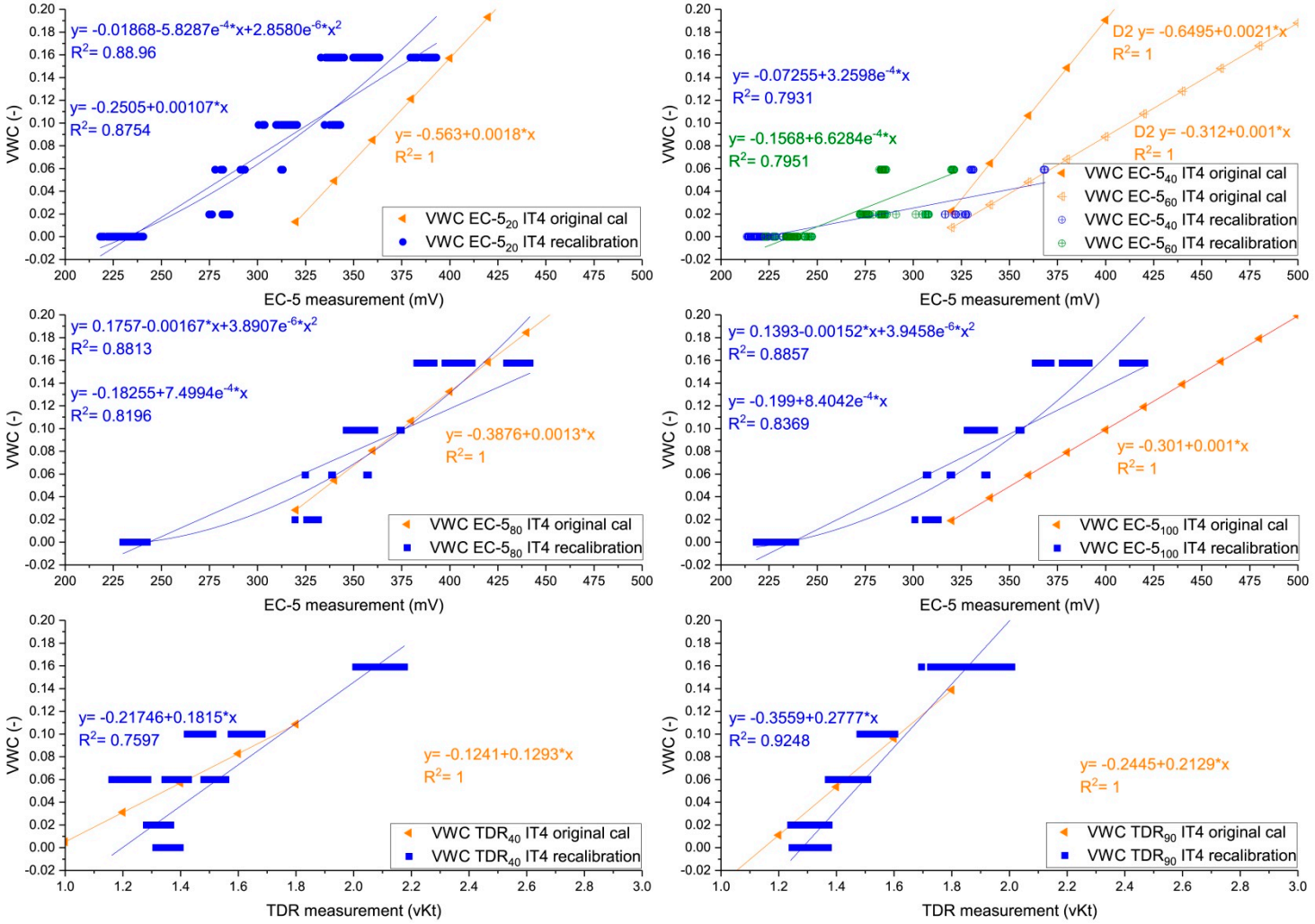

Figure S14. Site-specific calibration for positive temperatures, IT4.

References

1. Buchheister, J.A. Verflüssigungspotenzial von reinem und siltigem Sand unter multiaxialer Belastung. Publication of the Institute of Geotechnical Engineering, 2012, Band 240. ETH Zürich, Zürich. Dr. Sc. ETH-Dissertation Nr. 18312.
2. Guldenfels, R. Die Alterung von Bahnschotter aus bodenmechanischer Sicht. Publication of the Institute of Geotechnical Engineering, 1995, Band 209. ETH Zürich, Zürich. Dr. Sc. ETH-Dissertation Nr. 11209.
3. Annan, A. P. GPR Methods for hydrogeological studies, *Hydrogeophysics* **2005**, 185-213.
4. Annan, A. P. Electromagnetic principles of ground penetrating radar; Ground penetrating radar: Theory and applications. Elsevier Science, Amsterdam, 2009.
5. Neal, A. Ground-penetrating radar and its use in sedimentology: principles, problems and progress. *Earth Sci. Rev.* **2004**, *66*(3-4), 261-330.
6. Topp, G. C.; Davis, J. L.; Annan, A. P. Electromagnetic determination of soil water content: measurements in coaxial transmission lines. *Water Resour. Res*. **1980**, 16 (3), 574–582.
7. Davis, J. L.; Annan, A. P. Ground-Penetrating Radar for High-Resolution Mapping of Soil and Rock Stratigraphy 1. *Geophys. Prospect.* **1989**, 37(5), 531-551.
8. Wobschall, D. A Frequency shift dielectric soil moisture sensor; IEEE Transactions on Geoscience Electronics 1978, 16. 112-118, doi: 10.1109/TGE.1978.294573
9. Pepin, S.; Livingston, N. J.; Hook, W. R. Temperature-dependent measurement errors in time domain reflectometry determinations of soil water. *Soil Sci. Soc. Am J.* **1995**, 59(1), 38-43.
10. Bogena, H. R.; Huisman, J. A.; Oberdörster, C.; Vereecken, H. Evaluation of a low-cost soil water content sensor for wireless network applications. *J. Hydrol*. **2007**, 344(1-2), 32-42.